



Understanding the origins of N₂O decomposition activity in Mn(Fe)CoAlO_x hydrotalcite derived mixed metal oxides



Magdalena Jabłońska^{a,b,*}, Miren Agote Arán^c, Andrew M. Beale^{c,d}, Gérard Delahay^e, Carolina Petitto^e, Marek Nocuń^f, Regina Palkovits^{a,b,*}

^a Institut für Technische und Makromolekulare Chemie, Chair of Heterogeneous Catalysis and Chemical Technology, RWTH Aachen University, Worringerweg 2, 52074, Aachen, Germany

^b Center for Automotive Catalytic Systems Aachen – ACA, RWTH Aachen University, Schinkelstr. 8, 52062 Aachen, Germany

^c Department of Chemistry, University College London, 20 Gordon Street, London, WC1H 0AJ, UK

^d Research Complex at Harwell, Rutherford Appleton Laboratories, Didcot, Oxon, OX11 0FA, UK

^e Institut Charles Gerhardt de Montpellier, 240 avenue du Professeur Emile Jeanbrau, 34296, Montpellier Cedex 5, France

^f Faculty of Material Science and Ceramics, AGH University of Science and Technology, Mickiewicza 30, 30-059, Kraków, Poland

ARTICLE INFO

Keywords:

Hydrotalcite-like compounds
Mixed metal oxides
Cobalt
N₂O decomposition
In situ XAFS

ABSTRACT

The catalytic decomposition of N₂O was studied over a series of calcined Mn(Fe)CoAl hydrotalcite-like compounds. The precursors were prepared by coprecipitation and characterized by XRD and TGA. The mixed metal oxides derived after calcination at 600 °C were characterized by XRD, N₂ adsorption, H₂-TPR and XPS. Moreover, in situ XAFS measurements over selected mixed metal oxides were performed. Such investigations under relevant reaction conditions are rare, while a comprehensive understanding of the involved active species may facilitate a knowledge-based catalyst optimization. The activity of the CoAlO_x (Co/Al = 3/1, mol.%) catalyst varied depending on the loading of Mn or Fe (0.0575, 0.0821, 0.1150, 0.1725, 0.2300, mol.%). In the investigated series, Mn_{0.1725}Co₃Al₁O_x reached the highest activity with T₅₀ of about 305 and 376 °C under N₂O/N₂ and N₂O,NO,O₂/N₂ feed, respectively. In situ X-ray absorption experiments over Mn_{0.1725}Co₃Al₁O_x suggested that Mn_xCo_yO₄ spinels undergo reduction to CoO and MnO upon heating up to 600 °C in He. Under N₂O/He conditions, initial reoxidation of cobalt species began at 350 °C. The lower activity obtained for Fe_{0.1725}Co₃Al₁O_x is explained by the fact that the majority of Fe was not incorporated into the Co₃O₄ structure but instead formed less reactive iron oxide clusters.

1. Introduction

The catalytic decomposition of N₂O (deN₂O) can be considered as one of the best available technologies for N₂O abatement from nitric acid production, which is one of its major industrial sources. A broad collection of catalysts has been investigated at temperatures below 450–500 °C [1]. As implied by the published results, hydrotalcite derived mixed metal oxides present high activity for deN₂O even in the presence of H₂O, O₂, SO₂ and/or NO_x. The hydrotalcite-like compounds with a general formula of M_{1-x}M³⁺_x(OH)₂(Aⁿ⁻)_{x/n}mH₂O, where M²⁺ and M³⁺ – bi- and trivalent metal cations, respectively, Aⁿ⁻ – an interlayer anion and x – M³⁺/(M³⁺ + M²⁺) with a value between 0.17–0.50 [2,3], serve as excellent precursors for the preparation of catalysts of the desired chemical and phase composition for deN₂O. Thermal decomposition of hydrotalcite-like compounds at middle

temperatures (≤ 600 °C) results in the formation of relatively high surface area mixed metal oxides with a high dispersion of introduced transition oxide metal species [4–6]. Recently, Jabłońska and Palkovits [1,7] reviewed hydrotalcite derived mixed metal oxides in deN₂O and concluded that the activity of the mixed metal oxides varied depending on the type and loading of the catalytically active metal, its oxidation state as well as dispersion and aggregation state, etc. The research of hydrotalcite derived mixed metal oxides focusses mainly on cobalt-based materials: CoAlO_x (e.g. [8,9]), Co(Mg)Mn(Al)O_x (e.g. [10–12]), CoMgAlO_x or CoCuMgAlO_x (e.g. [13]), etc. Kannan et al. [14–16] and furthermore Pérez-Ramírez et al. [8] found Co/Al with 3/1 M ratio as optimal hydrotalcite derived catalyst dedicated to deN₂O among catalysts varied between Co/Al = 3-1/1, mol.%. Co₃Al₁O_x reached 84% (WHSV = 60 L (h g)⁻¹ [15]) to 100% (WHSV = 120 L (h g)⁻¹ [8]) conversion at 450 °C. Kannan et al. [15,16] reported that the activity of

* Corresponding authors at: Institut für Technische und Makromolekulare Chemie, Chair of Heterogeneous Catalysis and Chemical Technology, RWTH Aachen University, Worringerweg 2, 52074, Aachen, Germany.

E-mail addresses: Jablonska@itm.rwth-aachen.de (M. Jabłońska), Palkovits@itm.rwth-aachen.de (R. Palkovits).

CoAlO_x mixed metal oxides correlated with the Co/Al bulk composition, but, an even better correlation in the activity was obtained with the Co^{2+} (generated by surface reduction and reconstruction) of mixed metal oxides, as determined by XPS. Obalová et al. [10,11,17] investigated numerous combinations of $\text{Co}(\text{Mg})\text{Mn}(\text{Al})\text{O}_x$ and found $\text{Co}_4\text{Mn}_1\text{Al}_1\text{O}_x$ as optimum catalyst for deN_2O (82–97% conversion at 450 °C, WHSV = 60 L (h g)⁻¹). The authors reported an optimum surface amount of $\text{Co}^{2+}/\text{Co}^{3+}$ and $\text{Mn}^{2+}/\text{Mn}^{3+}$ molar ratios at 1.13 and 2.27 by XPS. Moreover, as determined from H₂-TPR, $\text{Co}_4\text{Mn}_1\text{Al}_1\text{O}_x$ possessed an optimum number of components reducible in the temperatures of the maximum conversion of N_2O (between 350–450 °C) [11]. We note that to date there are no studies on hydrotalcite derived catalysts under reaction conditions available and as such insight into the active form of the catalyst is currently absent. Such information however, often provides a better understanding of what makes for a good or poor catalyst. Our present investigation focused on identifying the exact nature and behaviour of metal species in $\text{Mn}(\text{Fe})\text{CoAlO}_x$ mixed metal oxides applied to deN_2O using *in situ* XAFS supported by ex situ characterisation of precursors and/or mixed metal oxides using XRD, TG, N₂ adsorption and H₂-TPR, in order to explore additional structure-activity correlations.

2. Experimental

2.1. Catalyst preparation

A series of $\text{Mn}(\text{Fe})_n\text{Co}_3\text{Al}_1$ ($n = 0.0575, 0.0821, 0.1150, 0.1725, 0.2300$, mol.%) hydrotalcite-like compounds was prepared by coprecipitation. An aqueous solution containing appropriate amounts of following metal nitrates: $\text{Co}(\text{NO}_3)_2 \cdot 6\text{H}_2\text{O}$ (Roth), $\text{Al}(\text{NO}_3)_3 \cdot 9\text{H}_2\text{O}$ (Sigma), $\text{Mn}(\text{NO}_3)_2 \cdot 4\text{H}_2\text{O}$ (Roth), $\text{Fe}(\text{NO}_3)_3 \cdot 9\text{H}_2\text{O}$ (Roth) and 1 M NaOH (Chemsolute) was dropped simultaneously into a vigorously stirred aqueous solution containing a slight over-stoichiometric excess of Na_2CO_3 (Sigma) at 60 °C. The pH of the reaction mixture was maintained constant at 10.0 ± 0.2 throughout the whole synthesis by NaOH addition. The obtained suspension was aged at 60 °C for another 0.5 h after complete coprecipitation. The solid was filtered, washed carefully with distilled water and dried at room temperature. Finally, the prepared hydrotalcite-like compounds were crushed and calcined at 600 °C for 6 h with a heating ramp of 10 K min⁻¹ and in static air. The hydrotalcite derived mixed metal oxides were kept in a desiccator in order to avoid the reconstruction of the hydroxide-like structure. For catalytic experiments, a fraction of particle size in the range of 0.250–0.500 mm was used.

2.2. Catalyst characterization

The X-Ray diffraction (XRD) measurements of the all as-synthesized hydrotalcite-like compounds and mixed metal oxides formed by their thermal decomposition was performed on a Siemens D5000 XRD diffractometer using Cu-K α radiation ($\lambda = 1.54056 \text{ \AA}$, 45 kV, 40 mA).

The difference thermogravimetric analyses (DTG) of the hydrotalcite-like compounds (~20 mg) were carried out using a Netzsch STA 409C/CD operated under a flow of air (10 cm³ min⁻¹) in the temperature range of 30–1000 °C with a linear heating rate of 5 K min⁻¹.

The specific surface area (S_{BET}) of the mixed metal oxides was determined by low-temperature (~196 °C) N₂ sorption using a Quantachrome Quadrasorb SI. Prior to nitrogen adsorption the samples were outgassed at 250 °C for 12 h using a Quantachrome Flovac degasser. The specific surface area (S_{BET}) was calculated using the Brunauer-Emmett-Teller (BET) multiple point method in the p/p₀ range from 0.05 to 0.3.

The chemical analysis of mixed metal oxides was determined by ICP-MS using an Agilent Technologies 8800 Triple Quad spectrometer. Prior to measurement, the sample (50 mg) was dissolved in 6 cm³ mixture of concentrated acids (HCl:HNO₃, 1:1), and afterwards the resulting mixture was diluted with 64 cm³ deionized water before warming up to 40 °C for 24 h.

The redox properties of the selected mixed metal oxides were studied by the temperature-programmed reduction (H₂-TPR) using Quantachrome ChemBET Pulsar TPR/TPD. H₂-TPR runs for the samples (30 mg) were carried out starting from room temperature to 1000 °C with a linear heating rate of 10 K min⁻¹ and in a flow (25 cm³ min⁻¹) of 5.0 vol.% H₂/Ar. Water vapour was removed from effluent gas by means of a cold trap placed in an ice-water bath. The H₂ consumption was detected and recorded by TCD detector.

The X-ray photoelectron spectra (XPS) of selected mixed metal oxides were measured on a VSW spectrometer equipped with a hemispherical analyzer. The photoelectron spectra were measured using a magnesium Mg K α source ($E = 1253.6 \text{ eV}$). The base pressure in the analysis chamber during the measurements was $3 \cdot 10^{-6} \text{ Pa}$ and the spectra were calibrated on a main carbon C 1s peak at 284.6 eV. The composition and chemical surrounding of the sample surface were investigated based on the areas and binding energies of Co 2p, Mn 2p, Fe 2p, Al 2p, O 1s and C 1s photoelectron peaks. Mathematical analyses of the XPS spectra were carried out using the XPSpeak 4.1 computer software (RWM. Kwok, The Chinese University of Hong Kong).

The X-ray absorption spectra (XAS) of selected samples were collected *in situ* using the quartz capillary flow reactor cells and gas delivery systems available on the beamline, on station B18 at the Diamond Light Source synchrotron facility. The measurements were carried out using a Si(111) monochromator at the Co K-edge, Mn K-edge or Fe K-edge with the respective Co, Mn or Fe monometallic foils (10 μm) used as an energy calibrant for the monochromator. The catalyst diluted with SiO_2 (1:5) was sieved into 0.200–0.250 mm and placed into the reactor. Prior to the reaction the catalyst was outgassed at 600 °C for 1 h in a flow of pure He (10 cm³ min⁻¹), and subsequently cooled down to 100 °C. The reactant concentrations at the reactor inlet composed of $[\text{N}_2\text{O}] = 0.1 \text{ vol.\%}$ and He balance (10 cm³ min⁻¹). The temperature was raised in steps of 50–100 °C up to 600 °C. Each temperature was held for 30 min for spectra acquisition. Finally, the sample was cooled down to room temperature under pure He. X-ray absorption spectra at

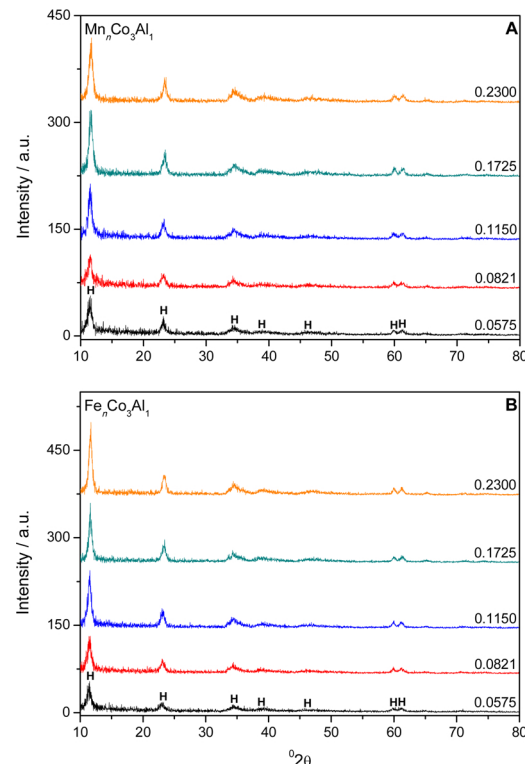


Fig. 1. X-ray diffraction patterns of $\text{Mn}(\text{Fe})_n\text{Co}_3\text{Al}_1$ ($n = 0.0575, 0.0821, 0.1150, 0.1725, 0.2300$, mol.%) hydrotalcite-like compounds; H – hydrotalcite-like phase.

Table 1

Lattice parameters of (Mn,Fe)CoAl hydrotalcite-like compounds and corresponding mixed metal oxides.

Hydrotalcite-like compounds	Cell parameter a/nm	Cell parameter c/nm	Crystallite size Da/nm	Crystallite size Dc/nm	Mixed metal oxides	Cell parameter a/nm	Crystallite size Da/nm
Co ₃ Al ₁	0.3079	2.2956	29	20	Co ₃ Al ₁ O _x	27	0.8093
Mn _{0.0575} Co ₃ Al ₁	0.3085	2.3065	33	22	Mn _{0.0575} Co ₃ Al ₁ O _x	32	0.8076
Mn _{0.0821} Co ₃ Al ₁	0.3086	2.3060	34	21	Mn _{0.0821} Co ₃ Al ₁ O _x	32	0.8083
Mn _{0.1150} Co ₃ Al ₁	0.3085	2.3006	25	24	Mn _{0.1150} Co ₃ Al ₁ O _x	27	0.8099
Mn _{0.1725} Co ₃ Al ₁	0.3080	2.2800	33	24	Mn _{0.1725} Co ₃ Al ₁ O _x	26	0.8079
Mn _{0.2300} Co ₃ Al ₁	0.3078	0.2790	27	24	Mn _{0.2300} Co ₃ Al ₁ O _x	26	0.8099
Fe _{0.0575} Co ₃ Al ₁	0.3085	2.3215	22	22	Fe _{0.0575} Co ₃ Al ₁ O _x	30	0.8073
Fe _{0.0821} Co ₃ Al ₁	0.3086	2.3100	39	26	Fe _{0.0821} Co ₃ Al ₁ O _x	33	0.8076
Fe _{0.1150} Co ₃ Al ₁	0.3085	2.3065	39	28	Fe _{0.1150} Co ₃ Al ₁ O _x	33	0.8093
Fe _{0.1725} Co ₃ Al ₁	0.3081	2.2839	34	28	Fe _{0.1725} Co ₃ Al ₁ O _x	30	0.8083
Fe _{0.2300} Co ₃ Al ₁	0.3081	2.2790	42	30	Fe _{0.2300} Co ₃ Al ₁ O _x	31	0.8096

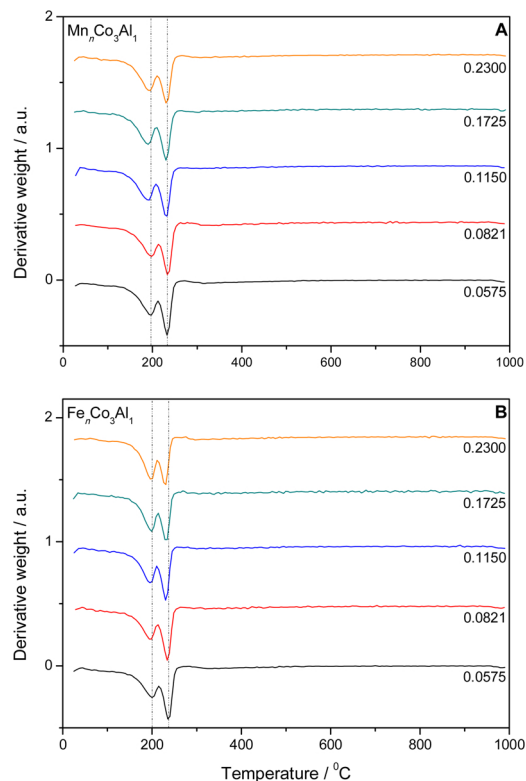


Fig. 2. DTG profiles of Mn(Fe)_nCo₃Al₁ ($n = 0.0575, 0.0821, 0.1150, 0.1725, 0.2300$, mol.%) hydrotalcite-like compounds; experimental conditions: mass of sample = 20 mg, flow of synthetic air = $10 \text{ cm}^3 \text{ min}^{-1}$, liner heating rate of 5 K min^{-1} .

appropriate K-edges were collected in fluorescence mode for 240 s for Co, Fe or Mn K-edges. At least three spectra for each sample were taken (and averaged) at room temperature, appropriate temperatures and after reaction at room temperature. CoO, Co₃O₄, FeO, Fe₂O₃, MnO₂ references were measured only at room temperature. The data were analysed using the Demeter software package [18,19]; the edge position was determined as the first maximum – after the pre-edge peak – of the derivative of the XANES spectra.

2.3. Catalytic tests

The catalytic activity and selectivity of the mixed metal oxides was evaluated in the N₂O decomposition. The catalytic experiments were carried out under atmospheric pressure in a fixed-bed flow microreactor of 6 mm internal diameter. Prior to the reaction the catalyst (350 mg) was outgassed at 600 °C for 1 h in a flow of pure N₂ ($100 \text{ cm}^3 \text{ min}^{-1}$). The reactant concentrations at the reactor inlet composed of: (i) [N₂O] = 0.1 vol.%, N₂

Table 2

Total mass loss of (Mn,Fe)CoAl hydrotalcite-like compounds, specific surface area (S_{BET}), sodium residuals of mixed metal oxides, and T_{50} of mixed metal oxides in N₂O/N₂, N₂O,NO,O₂/N₂* and N₂O,H₂O/He** gas mixtures.

Hydrotalcite-like compounds	Total mass loss/%	Mixed metal oxides	$S_{\text{BET}}/\text{m}^2 \text{ g}^{-1}$	Na/wt.%	$T_{50}/^\circ\text{C}$
Co ₃ Al ₁	32.62	Co ₃ Al ₁ O _x	82	1.4	352 ^a *409 ^a **549 ^b
Mn _{0.0575} Co ₃ Al ₁	31.90	Mn _{0.0575} Co ₃ Al ₁ O _x	59	0.7	317 ^a
Mn _{0.0821} Co ₃ Al ₁	31.54	Mn _{0.0821} Co ₃ Al ₁ O _x	57	1.3	332 ^a
Mn _{0.1150} Co ₃ Al ₁	30.53	Mn _{0.1150} Co ₃ Al ₁ O _x	61	1.0	320 ^a
Mn _{0.1725} Co ₃ Al ₁	30.89	Mn _{0.1725} Co ₃ Al ₁ O _x	76	2.3	305 ^a *376 ^a **528 ^b
Mn _{0.2300} Co ₃ Al ₁	31.03	Mn _{0.2300} Co ₃ Al ₁ O _x	65	0.8	316 ^a
Fe _{0.0575} Co ₃ Al ₁	31.43	Fe _{0.0575} Co ₃ Al ₁ O _x	56	0.8	356 ^a
Fe _{0.0821} Co ₃ Al ₁	31.34	Fe _{0.0821} Co ₃ Al ₁ O _x	53	0.8	325 ^a
Fe _{0.1150} Co ₃ Al ₁	31.10	Fe _{0.1150} Co ₃ Al ₁ O _x	54	1.6	333 ^a
Fe _{0.1725} Co ₃ Al ₁	30.27	Fe _{0.1725} Co ₃ Al ₁ O _x	54	0.9	327 ^a *380 ^a **549 ^b
Fe _{0.2300} Co ₃ Al ₁	31.00	Fe _{0.2300} Co ₃ Al ₁ O _x	50	0.9	355 ^a

^a 350 mg of catalyst, $100 \text{ cm}^3 \text{ min}^{-1}$ total flow.

^b 70 mg of catalyst, $75 \text{ cm}^3 \text{ min}^{-1}$ total flow.

balance, (ii) [N₂O] = 0.1 vol.%, [NO] = 0.03 vol.%, [O₂] = 4.5 vol.%, N₂ balance ($100 \text{ cm}^3 \text{ min}^{-1}$; WHSV = 17 L (h g)^{-1} , and were analyzed by infrared spectroscopy using a Perkin Elmer Spectrum Two equipped with a Pike 5 m heated gas cell. The temperature was raised in steps of $50 \text{ }^\circ\text{C}$ starting from 100 up to 600 °C. Each temperature was set constant for 0.5 h.

For selected material, additional tests were performed in the presence of water vapour. Such catalytic experiments were carried out under atmospheric pressure in a fixed-bed flow microreactor of 9 mm internal diameter. Prior to the reaction, the catalyst (70–150 mg) was activated at 580 °C for 0.5 h in a flow of pure He ($75 \text{ cm}^3 \text{ min}^{-1}$). After reactor cooled down, the following composition was applied: [N₂O] = 0.1 vol.%, ([H₂O] = 3.5 vol.%), He balance ($75 \text{ cm}^3 \text{ min}^{-1}$; WHSV = $30\text{--}64 \text{ L (h g)}^{-1}$), and were analyzed by a Pfeiffer Omnistar quadrupole mass spectrometer equipped with Channeltron and Faraday detectors (0–200 amu). Water vapour was added by means of a saturator whose temperature was controlled by a thermostat.

The conversion of N₂O (X(N₂O)) was estimated according to $X(\text{N}_2\text{O}) = ([\text{c}(\text{N}_2\text{O})_{\text{in}} - \text{c}(\text{N}_2\text{O})_{\text{out}}]/[\text{c}(\text{N}_2\text{O})_{\text{in}}] \times 100\%$, where: c(N₂O)_{in} and c(N₂O)_{out} – concentration of N₂O in the inlet gas, and concentration of N₂O in the outlet gas.

3. Results and discussion

Firstly, the structure of our precursors has been controlled to ensure that mixed metal oxide catalysts were issued from a material having the

same structure. Fig. 1 presents the XRD patterns of $\text{Mn}(\text{Fe})_n\text{Co}_3\text{Al}_1$ ($n = 0.0575, 0.0821, 0.1150, 0.1725, 0.2300$, mol.%) hydrotalcite-like compounds, exhibiting rhombohedral symmetry (space group R3m, 3R polytype) [20] with sharp and symmetrical reflections (0 0 3), (0 0 6), (1 1 0) and (1 1 3), and broad and asymmetrical reflections (0 1 2), (0 1 5) and (0 1 8). The intensity of the reflection corresponding to the hydrotalcite-like phase were very weak for samples with 0.0575 mol.% of Mn or Fe. However, the intensity of such phases increased with increasing loading of both transition metals. Table 1 summarizes the unit cell parameters of the hydrotalcite-like compounds and their derivatives. The cell parameters were calculated using the position of (1 0 1) reflection: $a = 2(d_{1\ 1\ 0})$ and positions of basal reflections: $c = [3(d_{0\ 0\ 3}) + 6(d_{0\ 0\ 6})]/2$. The lattice parameter a depends on the size of the cation in the brucite-like layers, while the parameter c refers to the interlayer thickness. The a value for $\text{Mn}(\text{Fe})_n\text{Co}_3\text{Al}_1$ ($n = 0.0575, 0.0821, 0.1150, 0.1725, 0.2300$, mol.%) hydrotalcite-like compounds varied only slightly with increasing Mn or Fe content and were close to that obtained for Co_3Al_1 . The a value depends mainly on the ionic radii of the cations in octahedral coordination (0.070 nm Co^{2+} , 0.070 nm Mn^{2+} and 0.070 nm Fe^{3+} [21], as cations of metal precursors). The c value of about 2.3 nm stays characteristic for hydrotalcite-like compounds containing carbonates located in the interlayer space [2]. The interlayer distances increased upon decreasing electronegativity of the cations: Co (1.70) > Fe (1.64) > Mn (1.60) > Al (1.47) (according to Allred-Rochow scale) [22]. The crystal size was calculated from the Scherrer equation $D = 0.89 \cdot \lambda / \beta \cdot \theta$, where D is the crystallite size, λ is the X-ray wavelength, β is the line broadening and θ is the Bragg angle. The Fe-containing materials revealed overall higher crystal size (with the exception of $\text{Fe}_{0.0575}\text{Co}_3\text{Al}_1$) than the corresponding MnCo_3Al_1 compounds.

Fig. 2 presents the DTG profiles of $\text{Mn}(\text{Fe})_n\text{Co}_3\text{Al}_1$ ($n = 0.0575, 0.0821, 0.1150, 0.1725, 0.2300$, mol.%) hydrotalcite-like compounds, while Table 2 gathers total mass loss of these materials. DTG profiles provided an additional proof of the presence of the hydrotalcite-like structure. The thermal decomposition of $\text{Mn}(\text{Fe})\text{-Co-Al}$ precursors proceeded in two main stages with total mass losses of about 30–33%. The first DTG minimum centered at about 190–200 °C corresponded to the removal of interlayer and weakly adsorbed water without collapse of the structure. The second peak located at about 230–235 °C appeared due to the dehydroxylation of the brucite-like layers and thermal decomposition of interlayer carbonates and nitrates (e.g. [5,6,20]). The temperatures and peak intensities did not change significantly among studied precursors, possibly due to small differences in the Mn or Fe loading as well as similar size of Mn^{2+} and Fe^{3+} (as cations of metal precursors) in octahedral coordination of 0.070 nm [21].

Fig. 3 shows the XRD patterns of calcined $\text{Mn}(\text{Fe})\text{-CoAl}$ hydrotalcite-like compounds. The hydrotalcite-like structure was completely destroyed upon heating at 600 °C resulting in the formation of a spinel phase with a range of possible composition, namely $\text{Co}_3\text{O}_4/\text{CoAl}_2\text{O}_4/\text{Co}_2\text{AlO}_4$ (with Bragg reflections located at 20 at 19, 31, 37, 39, 45, 56, 59, 65, 77°, e.g. [8,16]), exhibiting cubic symmetry (space group Fd3m) [23]. The lattice parameter a in the range of 0.8073–0.8099 nm was close to Co_3O_4 ($a = 0.8084$ nm). Mn- or Fe-containing materials did not reveal any diffraction characteristic of such transition metal oxides in the XRD patterns, which confirmed the absence of bigger crystallites. Crystal sizes of 26–33 nm were calculated from (3 1 1) brag reflection in the XRD patterns using the Scherrer equation.

Table 2 lists the specific surface area (S_{BET}) of the $(\text{Mn},\text{Fe})\text{-CoAlO}_x$ mixed metal oxides. S_{BET} for $\text{Co}_3\text{Al}_1\text{O}_x$ of $82 \text{ m}^2 \text{ g}^{-1}$, significantly decreased after introduction of Mn or Fe within its structure. A similar trend was observed for both series, i.e. decrease for materials with 0.0821 mol.% then increase up to 0.1725 mol.% and finally a drop in S_{BET} for materials with the highest loading of transition metal (0.2300 mol.%). However, slightly higher values for S_{BET} were reached over Mn-containing mixed metal oxides. Chemical analysis identified by ICP-MS evidenced sodium residual from preparation procedure up to 2.3 wt.%.

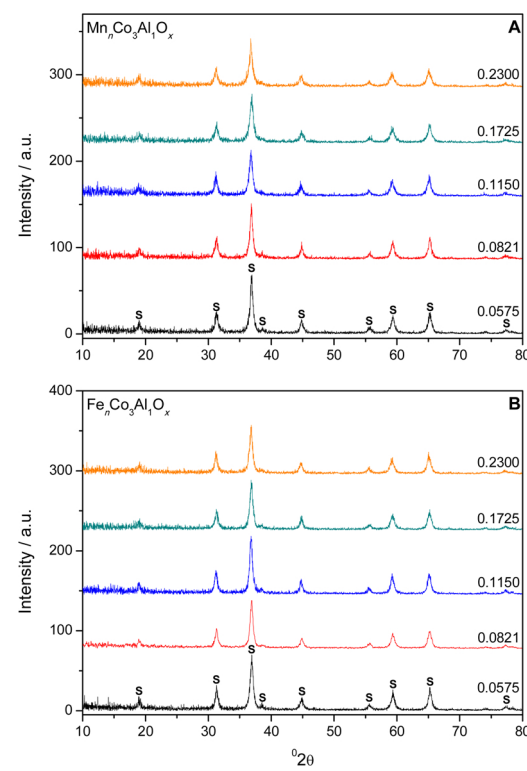


Fig. 3. X-ray diffraction patterns of $\text{Mn}(\text{Fe})_n\text{Co}_3\text{Al}_1\text{O}_x$ ($n = 0.0575, 0.0821, 0.1150, 0.1725, 0.2300$, mol.%) mixed metal oxides; S – $\text{Co}_3\text{O}_4/\text{CoAl}_2\text{O}_4/\text{Co}_2\text{AlO}_4$.

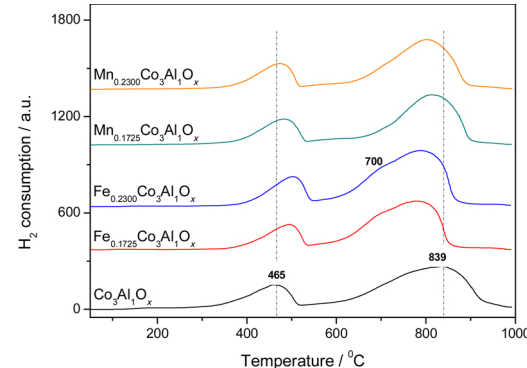


Fig. 4. $\text{H}_2\text{-TPR}$ profiles of selected $\text{Co}_3\text{Al}_1\text{O}_x$ and $\text{Mn}(\text{Fe})_n\text{Co}_3\text{Al}_1\text{O}_x$ ($n = 0.1725, 0.2300$, mol.%) mixed metal oxides; experimental conditions: mass of catalysts = 30 mg, $[\text{H}_2] = 5.0$ vol.%, $[\text{Ar}] = 95.0$ vol.%, flow rate = $25 \text{ cm}^3 \text{ min}^{-1}$, linear heating of 5 K min^{-1} .

Fig. 4 presents the $\text{H}_2\text{-TPR}$ profiles for $\text{Co}_3\text{Al}_1\text{O}_x$ and selected $\text{Mn}(\text{Fe})_n\text{Co}_3\text{Al}_1\text{O}_x$ ($n = 0.1725, 0.2300$, mol.%) mixed metal oxides. The $\text{H}_2\text{-TPR}$ profile for Co_3Al material revealed the presence of two main reduction peaks, with maxima centered at around 465 and 839 °C. The peak at lower temperature appeared due to the complete reduction of Co_3O_4 to metallic cobalt [24–26] while the high temperature reduction peak was related to the reduction of cobalt in $\text{Co}_2\text{AlO}_4/\text{CoAl}_2\text{O}_4$ [27]. $\text{Mn}(\text{Fe})_n\text{Co}_3\text{Al}_1\text{O}_x$ ($n = 0.1725, 0.2300$, mol.%) revealed similar $\text{H}_2\text{-TPR}$ profiles to $\text{Co}_3\text{Al}_1\text{O}_x$. However, the modification of Co_3Al with Mn or Fe influenced its redox properties, i.e. the position of the first reduction peaks shifted to higher temperatures for Mn- or Fe-doped materials than for $\text{Co}_3\text{Al}_1\text{O}_x$, while the position of the second peak shifted to lower temperatures, indicating depressed reducibility of Co_3O_4 and improved reducibility of cobalt in Co_2AlO_4 and CoAl_2O_4 . Such an effect was more

Table 3

Amount of H₂ consumed during H₂-TPR measurements (H₂ uptake), the peaks positions, their binding energy, peak area, full width at half maximum (FWHM) and O_α/(O_β + O_γ) molar ratio of mixed metal oxides.

Mixed metal oxides	H ₂ uptake ^a /mmol g ⁻¹	A ^b /A ^c /a.u.	Position Co 2p _{3/2} *O 1 s ■Mn 2p _{3/2} □Fe 2p _{3/2}	FWHM /eV	Area /a.u.	O _α /(O _β + O _γ) ^d
Co ₃ Al ₁ O _x	13.16 3.47 ^b 9.69 ^c	0.36	780.35 786.26 802.84 *527.07 *528.77 *530.38 *531.91	4.09 7.90 6.75 1.72 1.92 2.08 2.10	11998 4073 2239 462 2066 6369 2697	0.23
Mn _{0.1725} Co ₃ Al ₁ O _x	12.13 3.14 ^b 8.99 ^c	0.35	781.63 785.80 804.53 *528.51 *530.07 *531.72 *533.41 ■643.03	3.79 8.90 8.64 1.43 2.09 2.25 1.95 4.00	8333 2826 1134 239 2126 7926 2106 1080	0.21
Fe _{0.1725} Co ₃ Al ₁ O _x	12.63 2.75 ^b 9.88 ^c	0.28	779.63 784.18 802.17 *526.58 *528.37 *529.81 *531.28 □710.44	3.94 8.19 8.64 1.63 2.20 2.04 2.06 5.20	7137 2085 1244 324 2077 4523 1933 956	0.32

^a Calculated by equation: Y = 9E-09X + 2E-07, R² = 0.9996, and X, Y referred to the area of each reduction peak and the H₂ consumption, respectively.

^b In the region 50–530 °C.

^c In the region 530–1000 °C.

^d Estimated from the integrated area of the respective XPS peaks.

visible for FeCoAlO_x. Additionally, for the Fe-containing samples a broad shoulder appeared at about 700 °C that could be ascribed either to a partial reduction of cobalt in Co₂AlO₄ and CoAl₂O₄ or to reduction of iron oxide species [4,5]. Taking into account, the lower loading of Mn or Fe introduced into Co₃Al₁O_x in comparison to the content of cobalt and aluminum, the first assumption seems more likely. Thus, also reduction of manganese oxide species was not distinguished. Nevertheless, the up-shifting of H₂-TPR peak of Co₃O₄ suggested that Mn and Fe have to be incorporated within the spinel structure.

Table 3 summarizes H₂-TPR data of the studied materials. The H₂ uptake varied in the range of 2.75–3.47 mmol g⁻¹ in the temperature range of 150–530 °C (where N₂O decomposition proceeded). Furthermore, analysis of reduction peak areas (A^b/A^c, estimated from the integrated areas of the respective H₂-TPR peaks) revealed a comparable ratio (0.28 to 0.36) across the samples. Due to different oxidation states of metal oxide species in spinel forms, the calculations of the H₂ uptake based on materials composition are at best speculative. **Fig. 5** shows the Co 2p, O 1s, Mn 2p and Fe 2p XPS spectra of Co₃Al₁O_x and Mn(Fe)_{0.1725}Co₃Al₁O_x, while **Table 3** summarizes the peaks positions, their binding energy, peak area, full width at half maximum (FWHM) and O_α/(O_β + O_γ) molar ratio. The Co 2p XPS spectra exhibited two main peaks characterized by binding energy in the ranges of 781.6–779.6 and 796.9–795.0 eV corresponding to the Co2p_{3/2} and 2p_{1/2} spin-orbit peaks respectively [28]. Thus, since the spin-orbit values for the tested materials have varied in the range of 15.3–15.4 eV, we concluded that mainly Co₃O₄ (spin-orbit value of 15.2 eV) together with CoAl₂O₄ (as minor compound; spin-orbit value of 15.9 eV) was present on the catalyst surface [28–30]. Considering that Mn or Fe are present only in small amounts, determination of their chemical state in the measured Mn(Fe)_{0.1725}Co₃Al₁O_x based on the position of the binding energy is again largely speculative. Furthermore, Mn or Fe may be present in several chemical states with the overlapping spectra, which are close in energy [11,31]. The O 1s spectra were deconvoluted to lattice oxygen –

O_α, surface adsorbed oxygen, OH groups and oxygen vacancies – O_β and adsorbed molecular water – O_γ [32]. Additional low peaks at about 527–528 eV appeared possibly due to the differential charging of the materials [33]. The molar ratio of O_α/(O_β + O_γ) varied in the range of 0.21–0.32.

Fig. 6 shows the XANES spectra of Mn(Fe)_{0.1725}Co₃Al₁O_x mixed metal oxides. In comparison to the Co₃O₄ reference spectrum (Co K-edge), the spectrum of Mn_{0.1725}Co₃Al₁O_x at room temperature showed a more intense pre-edge peak which could be rationalized as being caused by a greater proportion of Co ions with a non-centrosymmetric geometry in this sample. Furthermore, an adsorption edge at lower energies – 7717.63 eV for Co₃O₄ and 7717.100 eV for Mn_{0.1725}Co₃Al₁O_x at room temperature, indicated a lower overall Co oxidation state (**Fig. 6A**). This suggested the presence of a CoAl₂O₄ type spinel where the substitution of Co³⁺ by Al³⁺ in the octahedral position leads to a higher contribution of Co²⁺ Td. Indeed, it has previously been shown that CoAl₂O₄ type spinel phase can form at temperatures as low as 390 °C [34]. The Mn K-edge spectra acquired at room temperature (**Fig. 6B**) closely resembled that of a Mn₃O₄ spinel reported previously [35]. To date no XAFS data exists concerning mixed Mn and Co spinels although a detailed XRD/vibrational spectroscopic study of Co/Mn substitution suggests that such phases can readily be formed and therefore a mixed Mn_xCo_yO₄ and/or Mn_xCo_yAl₂O₄ could be present in the Mn_{0.1725}Co₃Al₁O_x sample [36]. For Fe_{0.1725}Co₃Al₁O_x mixed metal oxides measured at room temperature, Co K-edge XANES revealed comparable Co speciation to the Mn-containing sample (**Fig. 6E**). Nevertheless, the Fe XANES spectrum closely resembled that of α-Fe₂O₃ (**Fig. 6F**), suggesting that unlike Mn, Fe did not incorporate so readily into the Co₃O₄ structure. In agreement, the shift to higher temperatures of Co₃O₄ reduction peak in the H₂-TPR profile suggested that small amounts of iron must have incorporated into the spinel structure thereby affecting its redox properties.

Changes occurring in Mn_{0.1725}Co₃Al₁O_x mixed metal oxides, during thermal treatment (up to 600 °C) in the presence of He and N₂O/He,

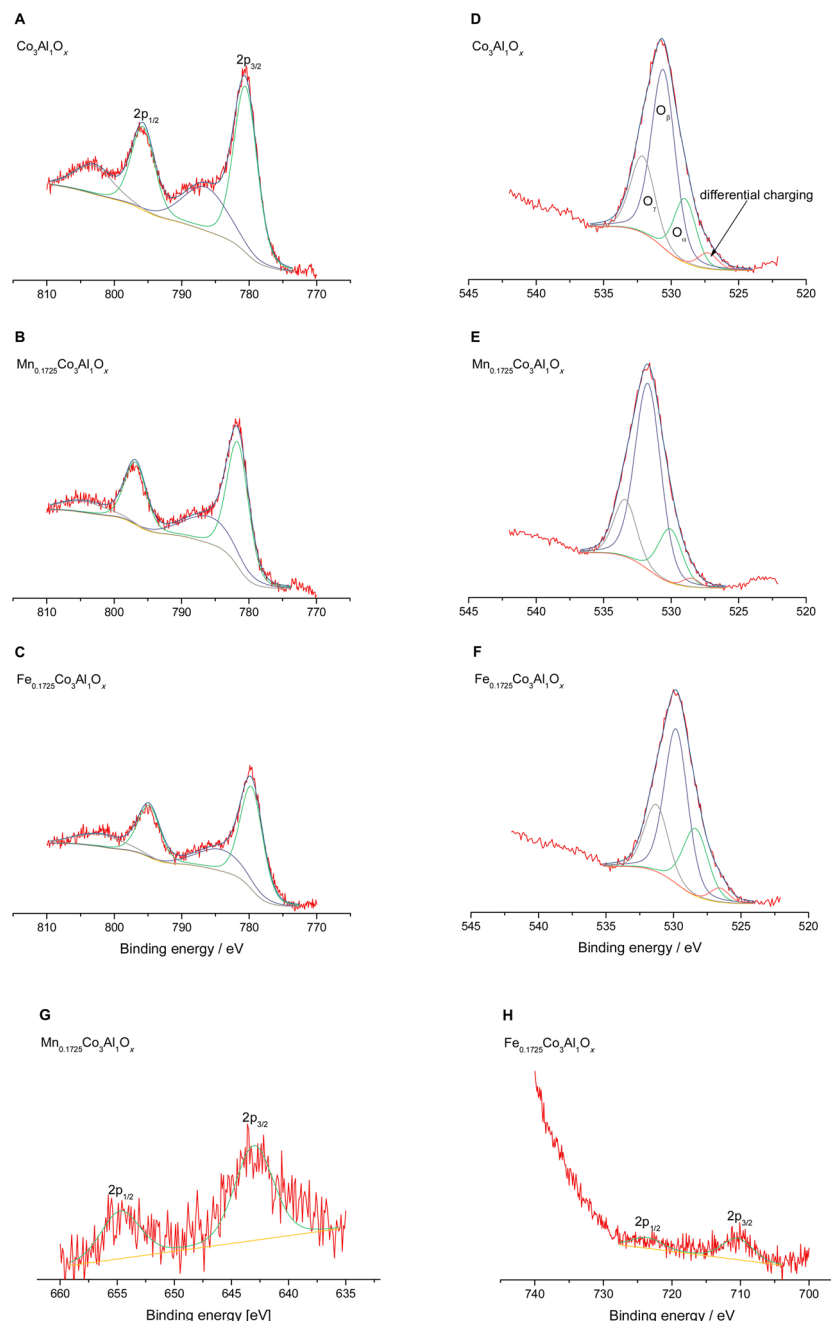


Fig. 5. XPS spectra of $\text{Co}_3\text{Al}_1\text{O}_x$ and $\text{Mn}(\text{Fe})_{0.1725}\text{Co}_3\text{Al}_1\text{O}_x$ mixed metal oxides; Co 2p (A–C), O 1s (D–F), Mn 2p (G) and Fe 2p (H).

were followed by studying the Co and Mn K-edge XANES spectra. A shift in the Co absorption edge to lower energies as well as a decrease in the pre-edge intensity were observed upon He treatment at 600 °C, which is indicative of a decrease in the nominal valence of Co in the material (Fig. 6A). The spectra resembled that of the CoO reference constituted by Co^{2+} in an octahedral environment. However, the higher pre-edge intensity of the sample when compared to $\text{CoO}/\text{Co}_3\text{O}_4$ suggested some Co^{2+} was still present in a tetrahedral environment. Considering the H_2 -TPR results pertaining to the reducibility of both cobalt oxide species present in the catalyst, it seems that $\text{Mn}_x\text{Co}_y\text{O}_4$ is reduced to $(\text{Mn})\text{CoO}$ while CoAl_2O_4 , with Co^{2+} in a tetrahedral environment, remained unchanged. EXAFS k -plots for Co and Mn in $\text{Mn}_{0.1725}\text{Co}_3\text{Al}_1\text{O}_x$ before and after reduction are shown in Fig. 1S in the Supplementary information. At room temperature the Mn and Co fine structure resembled closely the Co_3O_4 reference while in the reduced sample the fine structure is similar to CoO. This further confirms the

presence of the initial spinel environment for both Mn and Co and that in both cases this evolves into the rock salt M^{2+}O phase. Similar to Co, Mn also undergoes reduction upon activation in He at 600 °C; the reduced spectra resembling features of MnO [35]. Finally, in the presence of $\text{N}_2\text{O}/\text{He}$, both Co and Mn oxide species reoxidized to their initial state. Fig. 6C and D show the temperature dependence of this reoxidation process; the spectral changes were observed at 300–450 °C temperature range which coincided with the temperature needed to obtain full N_2O conversion. MnO appeared easier to reoxidize than CoO since the spectral changes in Mn K-edge XANES commenced at 300 °C while changes in Co K-edge occurred at 350 °C.

Furthermore, the changes in the oxidation state of Co at different reaction stages in $\text{Mn}_{0.1725}\text{Co}_3\text{Al}_1\text{O}_x$ were studied by the investigation of the position of the absorption edge (defined as the first maximum of the derivative plot beyond the pre-edge peak). Table 4 presents the Co K-edge absorption positions relative to Co foil ($\Delta E = E_{\text{sample}} - E_{\text{foil}}$) of

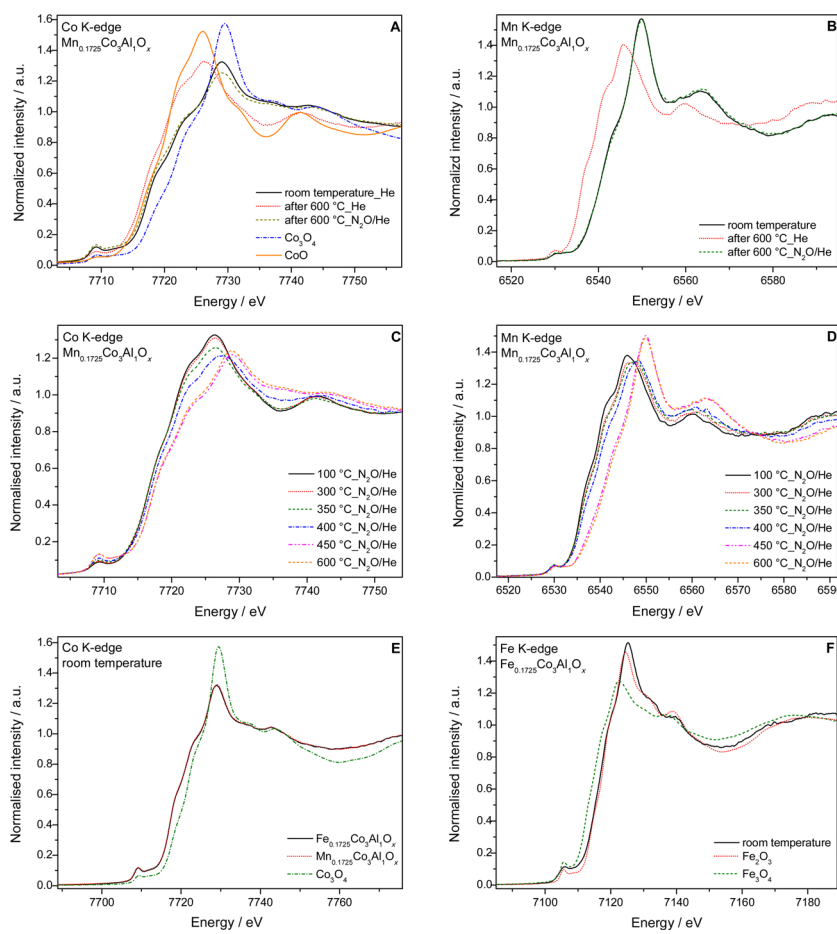


Fig. 6. In situ XANES spectra of A) Co K-edge for Mn_{0.1725}Co₃Al₁O_x at different reaction stages and Co references; B) Mn K-edge for Mn_{0.1725}Co₃Al₁O_x sample acquired at different stages of reaction; C) Co K-edge during the temperature ramp under N₂O; D) Mn K-edge during the temperature ram under N₂O; E) Co K-edge for Mn_{0.1725}Co₃Al₁O_x, Fe_{0.1725}Co₃Al₁O_x and Co₃O₄ reference at room temperature; and F) Fe K-edge for Fe_{0.1725}Co₃Al₁O_x and references.

Table 4

Co K-edge energy position relative to Co foil (E₀) for Mn_{0.1725}Co₃Al₁O_x at room temperature, after reduction under He and after reoxidation under N₂O/He at 600 °C as well as references at room temperature.

Mixed metal oxides	ΔE/eV	References	ΔE/eV
Mn _{0.1725} Co ₃ Al ₁ O _x		room temperature	
room temperature	8.1	CoO	7.4
after He 600 °C	7.4	Co ₃ O ₄	8.5
after N ₂ O/He 600 °C	8.1		

Table 5

Coordination number (CN), bond distances between adsorbed and backscatter atoms (R), inner potential correction to account for the difference in the inner potential between the sample and the reference compound (E), Debye-Waller factor ($2\sigma^2$), and residual factor (Rf) of Mn_{0.1725}Co₃Al₁O_x mixed metal oxides.

Mixed metal oxides	Shell Co-O	CN	R/nm	ΔE ₀ /eV	$10^{2*}\sigma^2/\text{nm}^2$	R _f /%
Fe _{0.1725} Co ₃ Al ₁ O _x						
room temperature He ^a	4.0	0.191	3.75	0.049	2.63	
Mn _{0.1725} Co ₃ Al ₁ O _x						
room temperature He ^a	4.0	0.191	3.05	0.041	2.65	
after He 600 °C ^b	6.0	0.206	-0.04	0.134	4.53	
after N ₂ O/He 600 °C ^a	4.0	0.191	3.28	0.067	3.79	

^a fitting of the spectra collected at room temperature.

^b fitting of the spectra collected at 100 °C.

Mn_{0.1725}Co₃Al₁O_x at different stages of the experiment as well as the ΔE of Co₃O₄ and CoO references. Again, the ΔE of the sample after treatment with He at 600 °C was comparable to CoO. While the reoxidation, under N₂O/He conditions, leads to the recovery of its initial oxidation

state. **Table 5** lists the results of the curve-fitting analysis for the first coordination shell. First shell quick fit analysis of the EXAFS was carried out to gain insight into the average Co–O distances and coordination numbers. The fitting was performed for the Co K-edge spectra of Mn_{0.1725}Co₃Al₁O_x collected at room temperature prior to the activation, for the spectra collected after the activation in He (once cooled down at 100 °C under He) and for the spectra collected at room temperature after the N₂O/He treatment at 600 °C. For comparison, Co K-edge spectra of Fe_{0.1725}Co₃Al₁O_x at room temperature (prior thermal treatments) was also fitted. The results revealed higher Co–O bond distances of 206 nm for Mn_{0.1725}Co₃Al₁O_x after activation with He at 600 °C. Due to the presence of mixed sites and slightly higher temperature in the spectra acquisition of the preactivated sample, the DWF and CN values become meaningless; nonetheless, the bond length, being less affected by such factors, suggests the presence of a CoO type structure with Co²⁺ Oh. Otherwise, Mn_{0.1725}Co₃Al₁O_x at room temperature or in the presence of N₂O/He at 600 °C showed a shorter Co–O of 0.191 nm, corresponding mainly to the presence of a spinel phase. As expected from XANES, the Co–O shell fitting gave very similar results for Mn_{0.1725}Co₃Al₁O_x and Fe_{0.1725}Co₃Al₁O_x at room temperature.

Fig. 7 presents the results of catalytic tests performed over Mn (Fe)_nCo₃Al₁O_x ($n = 0.0575, 0.0821, 0.1150, 0.1725, 0.2300$, mol.%), while **Table 2** lists temperatures necessary to obtain 50% N₂O conversion (T₅₀). The particle size of 0.250–0.500 mm of our samples used for the catalytic measurements was in the same scale order than the particle size of the samples of the study reported by Klyushina et al. [23], who reported the absence of internal and external diffusion limitations. Moreover, the reactor diameter and the catalyst bed length criteria requirement were checked. D(reactor diameter)/dp(particle diameter ≈ 16 was above) and L (catalyst bed length)/dp was superior to 50. Therefore, we can certify that the catalytic reactions were realized in kinetic regime. The N₂O conversion

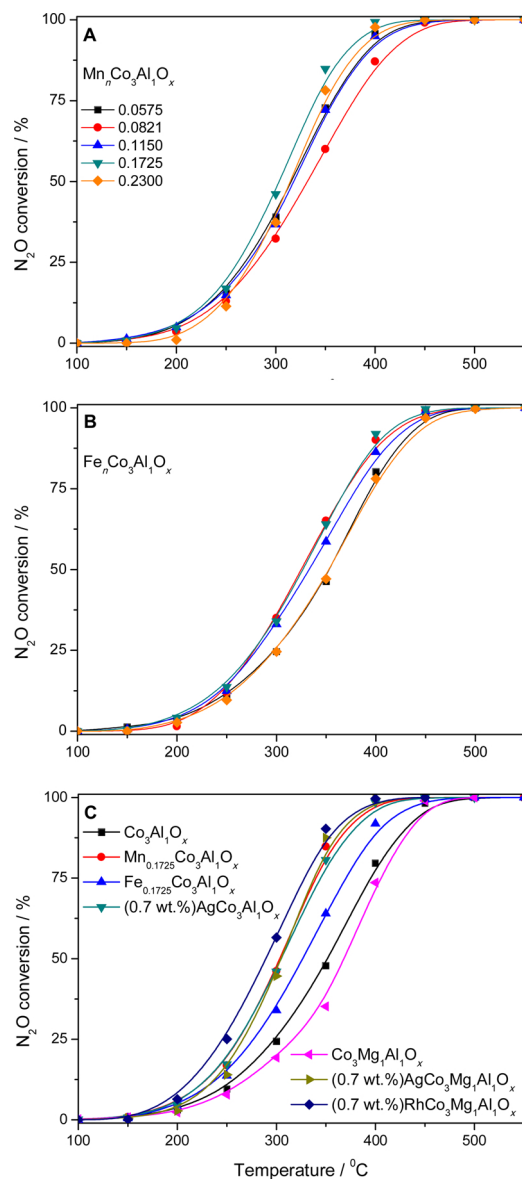


Fig. 7. Results of catalytic tests performed over $\text{Co}_3\text{Al}_1\text{O}_x$, $\text{Mn}(\text{Fe})_n\text{Co}_3\text{Al}_1\text{O}_x$ ($n = 0$, 0.0575, 0.0821, 0.1150, 0.1725, 0.2300) and (0.7 wt.%)Ag(Rh) $\text{Co}_3(\text{Mg}_1)\text{Al}_1\text{O}_x$ mixed metal oxides; reaction conditions: mass of catalysts = 350 mg, $[\text{N}_2\text{O}] = 0.1 \text{ vol.}\%$, N_2 balance, total flow rate = $100 \text{ cm}^3 \text{ min}^{-1}$, WHSV of $17 \text{ L} (\text{h g})^{-1}$.

from the reaction mixture started at about 150–200 °C, while full conversion was reached at about 450–500 °C for all tested materials. $\text{Co}_3\text{Al}_1\text{O}_x$ reached T_{50} at about 352 °C with the full conversion at 500 °C. Incorporation of Mn or Fe into $\text{Co}_3\text{Al}_1\text{O}_x$ structure improved the catalytic activity of mixed metal oxides. An exception was $\text{Fe}_{0.2300}\text{Co}_3\text{Al}_1\text{O}_x$, which showed catalytic activity similar to $\text{Co}_3\text{Al}_1\text{O}_x$. The reproducibility of our catalytic tests was confirmed by repeated measurements. The activity differentiated among tested materials however showed no clear trend and was neither related to the Mn or Fe nor Na (up to 2.3 wt.%) content. Alkali metals (e.g. Na, K, Li) can act as basic centres and influence catalytic activity. For example, Obalová et al. [12] pointed out that 1.15 wt.% of Na introduced by impregnation already slightly enhanced activity of $\text{Co}_4\text{MnAlO}_x$. However, materials with Na loaded by impregnation were reported to stronger facilitate N_2O decomposition than when Na was present after preparation [37,38]. The optimum amount of deposited Na varied also depending on the applied mixed metal oxides: 0.75 wt.% for $\text{Co}_{2.5}\text{Rh}_{0.05}\text{Al}_1\text{O}_x$ [38], 1.5 wt.% for $\text{Co}_3\text{Al}_1\text{O}_x$ [39] or 1.4 wt.% for

$\text{Co}_4\text{Mn}_1\text{Al}_1\text{O}_x$ [40]. Farris et al. [41] found out that an optimum Na residual content in the range of 3.0–6.0 wt.% in CoAlO_x was supposed to promote the decomposition of N_2O facilitating over 80% conversion at 475 °C. Doping with 1.0–2.0 wt.% of Na resulted in comparable results. In our case the amount of residual Na varied significantly from 0.7 up to 2.3 wt.% among samples despite application of the same material preparation procedure (including washing step). At this stage, it is not possible to precisely justify the influence of residual Na on materials activity in de N_2O . Certainly, further research should be carried out in order to clarify these remarkable observations over investigated $(\text{Mn},\text{Fe})\text{CoAlO}_x$ mixed metal oxides, considering also the synergistic effect of Mn(Fe) and residual Na on the catalytic activity.

The highest activity among tested materials reached $\text{Mn}_{0.1725}\text{Co}_3\text{Al}_1\text{O}_x$ with T_{50} at 305 °C and full conversion at 400 °C. Furthermore, $\text{Mn}_{0.1725}\text{Co}_3\text{Al}_1\text{O}_x$ possessed comparable activity to the Ag-doped catalysts – (0.7 wt.%)Ag $\text{Co}_3(\text{Mg}_1)\text{Al}_1\text{O}_x$, and only slightly lower activity than the (0.7 wt.%)Rh $\text{Co}_3\text{Mg}_1\text{Al}_1\text{O}_x$, reported as one of the most active and stable hydrotalcite derived mixed metal oxides in the N_2O decomposition with excellent activity and stability performance [7,42]. Catalytic tests were carried out under the same reaction conditions (Fig. 7C). Details regarding preparation, characterization and discussion of activity of both Ag- and Rh-containing mixed metal oxides were reported in our previous studies [43].

$\text{Co}_3\text{Al}_1\text{O}_x$ and $\text{Mn}(\text{Fe})_{0.1725}\text{Co}_3\text{Al}_1\text{O}_x$ were also tested in the presence of NO and O₂ (350 mg of catalyst, $100 \text{ cm}^3 \text{ min}^{-1}$ total flow). $\text{Mn}_{0.1725}\text{Co}_3\text{Al}_1\text{O}_x$ presented T_{50} of 376 °C, thus temperature of about 70 °C higher than for tests without NO and O₂. Slightly lower activity above 350 °C was obtained over $\text{Fe}_{0.1725}\text{Co}_3\text{Al}_1\text{O}_x$ with T_{50} at 380 °C. Furthermore, for practical applications, $\text{Co}_3\text{Al}_1\text{O}_x$ and $\text{Mn}(\text{Fe})_{0.1725}\text{Co}_3\text{Al}_1\text{O}_x$ were tested in the presence of H₂O (70 mg of catalyst, $75 \text{ cm}^3 \text{ min}^{-1}$), as displayed on Fig. 2SA. $\text{Mn}_{0.1725}\text{Co}_3\text{Al}_1\text{O}_x$ showed the highest resistance to water vapour with T_{50} of 549 °C. Other materials presented significantly lower resistance to water vapour. Fig. 2SB presents the contribution of NO formation over $\text{Co}_3\text{Al}_1\text{O}_x$ and $\text{Mn}(\text{Fe})_{0.1725}\text{Co}_3\text{Al}_1\text{O}_x$. The highest amount of such by-product in N_2O decomposition appeared over $\text{Fe}_{0.1725}\text{Co}_3\text{Al}_1\text{O}_x$. For other materials the formation of NO did not exceed 15 ppm in the studied temperature range of 200–550 °C. Notably, for catalytic tests carried out in the presence of water vapour NO formation decreased. In Fig. 3S, time-on-stream tests were conducted to evaluate the stability of $\text{Co}_3\text{Al}_1\text{O}_x$ and $\text{Mn}(\text{Fe})_{0.1725}\text{Co}_3\text{Al}_1\text{O}_x$ at 450 °C. All materials showed stable conversion during the first 85 min in the $\text{N}_2\text{O}/\text{N}_2$ feed. Subsequently, after introduction of water vapour into the feed, the conversion of all materials significantly dropped reaching a stable level below 20%. However, switching from wet to a dry reaction mixture resulted in an increase in catalyst conversion back to the initial dry level. Thus, the introduction of H₂O into the feed did not result in an irreversible deactivation of the catalysts.

Obalová et al. [11] reported that the high activity of $\text{Co}_4\text{Mn}_1\text{Al}_1\text{O}_x$ hydrotalcite derived mixed metal oxides appeared due to an optimum content of components reducible in the temperatures of the maximum conversion of N_2O (between 350–450 °C). Analysis of our reduction peak areas showed similar ratio (0.28 to 0.36) across the samples. Crystal sizes were calculated from (3 1 1) brag reflection in the XRD patterns using the Scherrer equation; comparable results of 27, 26 and 30 nm for $\text{Co}_3\text{Al}_1\text{O}_x$, $\text{Mn}_{0.1725}\text{Co}_3\text{Al}_1\text{O}_x$ and $\text{Fe}_{0.1725}\text{Co}_3\text{Al}_1\text{O}_x$, respectively, discard size effects in the catalytic activity and selectivity. In addition, no significant effect of textural properties on the catalytic results was found (S_{BET} of 82, 76, $54 \text{ m}^2 \text{ g}^{-1}$ for $\text{Co}_3\text{Al}_1\text{O}_x$, $\text{Mn}_{0.1725}\text{Co}_3\text{Al}_1\text{O}_x$ and $\text{Fe}_{0.1725}\text{Co}_3\text{Al}_1\text{O}_x$, respectively). Although, the strength of lattice oxygen-metal bonds was reported to determine the catalysts activity in de N_2O [44], we did not observe clear correlation between $\text{O}_\alpha/(\text{O}_\beta + \text{O}_\gamma)$ molar ratio and catalytic activity/selectivity of mixed metal oxides. Mn in $\text{Mn}_{0.1725}\text{Co}_3\text{Al}_1\text{O}_x$ appeared incorporated within spinel structure; MnO and CoO phases present after activation reoxidize under $\text{N}_2\text{O}/\text{He}$ feed. Indeed this observation of Mn being

easier to oxidise back to 3+ than Co, yet harder to reduce to 2+ is completely consistent with the respective redox potentials of the two elements [45]. On that basis Fe in $\text{Fe}_{0.1725}\text{Co}_3\text{Al}_1\text{O}_x$ could play a similar role as Mn. Nevertheless, as most of the iron was not incorporated to the spinel but appeared as separate Fe_2O_3 phase, its effect on catalytic activity was less pronounced than for Mn in the $\text{Mn}_{0.1725}\text{Co}_3\text{Al}_1\text{O}_x$ sample. Accordingly, decomposition of N_2O over the tested mixed metal oxides followed the cationic redox mechanism [42–44], consisting of N_2O activation by electron transfer from metal sites and diffusive recombination of the surface oxygen intermediates into oxygen, concerted with the back electron transfer that restores the oxidation state of the active sites. The regeneration of the active sites through oxygen desorption is considered as the rate-determining step. In this context, Co oxidizes when N_2O is adsorbed and then Co is again reduced when O_2 is released. Thus, during reaction under $\text{N}_2\text{O}/\text{He}$ conditions, Co is continuously oxidizing and reducing. The doping, in particular Mn, may generate new redox sites on the surface or may enhance the oxygen desorption from cobalt sites. Taking into account the very weak amount of manganese added and the fact that manganese appeared incorporated within the structure, the latter assumption seems more likely. Further studies will certainly aim for a deeper understanding of the individual role of the catalyst components in de N_2O .

4. Conclusion

$\text{Mn}(\text{Fe})_n\text{Co}_3\text{Al}_1\text{O}_x$ ($n = 0.0575, 0.0821, 0.115, 0.1725$ and 0.2300 , mol %) hydrotalcite derived mixed metal oxides were synthesized by coprecipitation and subsequent calcination. The catalytic activity of $\text{Co}_3\text{Al}_1\text{O}_x$ mixed metal oxides was improved in de N_2O by incorporation of an appropriate amount of Mn or Fe. $\text{Mn}_{0.1725}\text{Co}_3\text{Al}_1\text{O}_x$ reached the highest activity with T_{50} of about 305 and 376°C under $\text{N}_2\text{O}/\text{N}_2$ and $\text{N}_2\text{O}, \text{NO}, \text{O}_2/\text{N}_2$ feed, respectively. The trend for catalytic conversion was $\text{Mn}_{0.1725}\text{Co}_3\text{Al}_1\text{O}_x > \text{Fe}_{0.1725}\text{Co}_3\text{Al}_1\text{O}_x > \text{Co}_3\text{Al}_1\text{O}_x$. Detailed evaluation of the active species was realized by an in situ XAFS study. Correlation of the catalytic data with the XAS results suggested that doping Co_3O_4 spinel by Mn(Fe) lead to a facilitated desorption of oxygen. The presence of Mn in the spinel structure seemed to provide active surface Co sites that release oxygen more easily. The lower activity of the $\text{Fe}_{0.1725}\text{Co}_3\text{Al}_1\text{O}_x$ mixed metal oxides was attributed to the fact that Fe did not incorporate so readily into the cobalt spinel structure forming less active iron oxide clusters instead.

Acknowledgements

Funded by the Excellence Initiative of the German federal and state Governments in the frame of the Center for Automotive Catalytic Systems Aachen (ACA) at RWTH Aachen University. The authors acknowledge the Diamond Light Source (project SP14834) for provision of beamtime on the B18 beamline, and Diego Gianolio for assistance in performing the XAFS measurements. The authors thank Andreas Holz for the assistance in preparation, characterization and catalytic tests.

Appendix A. Supplementary data

Supplementary material related to this article can be found, in the online version, at doi:<https://doi.org/10.1016/j.apcatb.2018.10.010>.

References

- [1] M. Jabłońska, R. Palkovits, Nitrogen oxide removal over hydrotalcite-derived mixed metal oxides, *Catal. Sci. Technol.* 6 (2016) 49–72.
- [2] F. Cavani, F. Trifirò, A. Vaccari, Hydrotalcite-type anionic clays: preparation, properties and applications, *Catal. Today* 11 (1991) 173–301.
- [3] A. Vaccari, Preparation and catalytic properties of cationic and anionic clays, *Catal. Today* 41 (1998) 53–71.
- [4] L. Chmielarz, A. Węgrzyn, M. Wojciechowska, S. Witkowski, M. Michalik, Selective catalytic oxidation (SCO) of ammonia to nitrogen over hydrotalcite originated Mg–Cu–Fe mixed metal oxides, *Catal. Lett.* 141 (2011) 1345–1354.
- [5] M. Jabłońska, L. Chmielarz, A. Węgrzyn, K. Guzik, Z. Piwowarska, S. Witkowski, R.I. Walton, P.W. Dunne, F. Kovanda, Thermal transformations of Cu-Mg (Zn)-Al (Fe) hydrotalcite-like materials into metal oxide systems and their catalytic activity in selective oxidation of ammonia to dinitrogen, *J. Therm. Anal. Calorim.* 114 (2013) 731–747.
- [6] M. Jabłońska, K. Nothdurft, M. Nocuń, V. Girman, R. Palkovits, Redox-performance correlations in Ag-Cu-Mg-Al, Ce-Cu-Mg-Al, and Ga-Cu-Mg-Al hydrotalcite derived mixed metal oxides, *Appl. Catal. B Environ.* 207 (2017) 385–396.
- [7] M. Jabłońska, R. Palkovits, It is no laughing matter: nitrous oxide formation in diesel engines and advances in its abatement over rhodium-based catalysts, *Catal. Sci. Technol.* 6 (2016) 7671–7687.
- [8] J. Pérez-Ramírez, J. Overeijnder, F. Kapteijn, J.A. Moulijn, Structural promotion and stabilizing effect of Mg in the catalytic decomposition of nitrous oxide over calcined hydrotalcite-like compounds, *Appl. Catal. B Environ.* 23 (1999) 59–72.
- [9] J. Pérez-Ramírez, F. Kapteijn, J.A. Moulijn, High activity and stability of the Rh-free Co-based ex-hydrotalcite containing Pd in the catalytic decomposition of N_2O , *Catal. Lett.* 60 (1999) 133–138.
- [10] L. Obalová, K. Jiráčková, F. Kovanda, K. Pacultová, Z. Lacný, Z. Mikulová, Catalytic decomposition of nitrous oxide over catalysts prepared from Co/Mg-Mn/Al hydrotalcite-like compounds, *Appl. Catal. B Environ.* 60 (2005) 289–297.
- [11] L. Obalová, K. Pacultová, J. Balabánová, K. Jiráčková, Z. Bastl, M. Valášková, Z. Lacný, F. Kovanda, Effect of Mn/Al ratio in Co-Mn-Al mixed oxide catalysts prepared from hydrotalcite-like precursors on catalytic decomposition of N_2O , *Catal. Today* 119 (2007) 233–238.
- [12] L. Obalová, K. Karásková, A. Wach, P. Kustrowski, K. Mamulová-Kutláková, S. Michalik, K. Jiráčková, Alkali metals as promoters in Co-Mn-Al mixed oxide for N_2O decomposition, *Appl. Catal. A Gen.* 462–463 (2013) 227–235.
- [13] L. Chmielarz, M. Rutkowska, P. Kuśtrowski, M. Drozdek, Z. Piwowarska, B. Dudek, R. Dziembaj, M. Michalik, An influence of thermal treatment conditions of hydrotalcite-like materials on their catalytic activity in the process of N_2O decomposition, *J. Therm. Anal. Calorim.* 105 (2011) 161–170.
- [14] J.N. Armor, T.A. Braymer, T.S. Farris, Y. Li, F.P. Petrocelli, E.L. Weist, S. Kannan, C.S. Swamy, Calcined hydrotalcites for the catalytic decomposition of N_2O in simulated process streams, *Appl. Catal. B Environ.* 7 (1996) 397–406.
- [15] S. Kannan, Decomposition of nitrous oxide over the catalysts derived from hydrotalcite-like compounds, *Appl. Clay Sci.* 13 (1998) 347–362.
- [16] S. Kannan, C.S. Swamy, Catalytic decomposition of nitrous oxide over calcined cobalt aluminium hydrotalcites, *Catal. Today* 53 (1999) 725–737.
- [17] F. Kovanda, T. Rojka, J. Dobrošová, V. Machovič, P. Bezdička, L. Obalová, K. Jiráčková, T. Grygar, Mixed oxides obtained from Co and Mn containing layered double hydroxides: preparation, characterization, and catalytic properties, *J. Solid State Chem.* 179 (2006) 812–823.
- [18] M. Newville, IFEFFIT: interactive XAFS analysis and FEFF fitting, *J. Synchrotron Radiat.* 8 (2001) 322–324.
- [19] B. Ravel, M. Newville, ATHENA, ARTEMIS, HEPHAESTUS: data analysis for X-ray absorption spectroscopy using IFEFFIT, *J. Synchrotron Radiat.* 12 (2005) 537–541.
- [20] S.P. Newman, W. Jones, P. O’Connor, D.N. Stamires, Synthesis of the 3R2 polytypite of a hydrotalcite-like mineral, *J. Mater. Chem.* 12 (2002) 153–155.
- [21] R.D. Shannon, Revised effective ionic radii and systematic studies of interatomic distances in halides and chalcogenides, *Acta Crystallogr. Sect. A Cryst. Phys. Diffraction. Theor. Gen. Crystallogr.* 32 (1976) 751–767.
- [22] A.L. Allred, E.G. Rochow, A scale of electronegativity based on electrostatic force, *J. Inorg. Nucl. Chem.* 5 (1958) 264–268.
- [23] A. Klyushina, K. Pacultová, K. Karásková, K. Jiráčková, M. Ritz, D. Fridrichová, A. Volodarskaja, L. Obalová, Effect of preparation method on catalytic properties of Co-Mn-Al mixed oxides for N_2O decomposition, *J. Mol. Catal. A Chem.* 425 (2016) 237–247.
- [24] L. Chmielarz, Z. Piwowarska, M. Rutkowska, M. Wojciechowska, B. Dudek, S. Witkowski, M. Michalik, Total oxidation of selected mono-carbon VOCs over hydrotalcite originated metal oxide catalysts, *Catal. Commun.* 17 (2012) 118–125.
- [25] T. Franken, R. Palkovits, Investigation of potassium doped mixed spinels $\text{Cu}_x\text{Co}_{3-x}\text{O}_4$ as catalysts for an efficient N_2O decomposition in real reaction conditions, *Appl. Catal. B Environ.* 176–177 (2015) 298–305.
- [26] L. Xue, C. Zhang, H. He, Y. Teraoka, Catalytic decomposition of N_2O over CeO_2 promoted Co_3O_4 spinel catalyst, *Appl. Catal. B Environ.* 75 (2007) 167–174.
- [27] E. Genty, J. Brunet, C. Poupin, S. Casale, S. Capelle, P. Massiani, S. Siffert, R. Cousin, Co-Al mixed oxides prepared via LDH route using microwaves or ultrasound: application for catalytic toluene total oxidation, *Catalysts* 5 (2015) 851–867.
- [28] I.A.P.S. Murthy, C.S. Swamy, Catalytic decomposition of 2-propanol on $\text{Co}_{1+x}\text{Al}_{2-x}\text{O}_4$ spinel system, *Catal. Lett.* 27 (1994) 103–112.
- [29] J.-Y. Luo, M. Meng, X. Li, X.-G. Li, Y.-Q. Zha, T.-D. Hu, Y.-N. Xie, J. Zhang, Mesoporous $\text{Co}_3\text{O}_4\text{-CeO}_2$ and $\text{Pd/Co}_3\text{O}_4\text{-CeO}_2$ catalysts: synthesis, characterization and mechanistic study of their catalytic properties for low-temperature CO oxidation, *J. Catal.* 254 (2008) 310–324.
- [30] Z. Zhu, G. Lu, Z. Zhang, Y. Guo, Y. Guo, Y. Wang, Highly active and stable $\text{Co}_3\text{O}_4/\text{ZSM}-5$ catalyst for propane oxidation: effect of the preparation method, *ACS Catal.* 3 (2013) 1154–1164.
- [31] P. Graat, M.A.J. Somers, Quantitative analysis of overlapping XPS peaks by spectrum reconstruction: determination of the thickness and composition of thin iron-oxide films, *Surf. Interface Anal.* 26 (1998) 773–782.
- [32] V.P. Santos, M.F.R. Pereira, J.J.M. Órfão, J.L. Figueiredo, The role of lattice oxygen on the activity of manganese oxides towards the oxidation of volatile organic compounds, *Appl. Catal. B Environ.* 99 (2010) 353–363.
- [33] M. Konsolakis, Z. Ioakimidis, T. Kraia, G.E. Marnellos, Hydrogen production by

ethanol steam reforming (ESR) over CeO₂ supported transition metal (Fe, Co, Ni, Cu) catalysts: insight into the structure-activity relationship, *Catalysts* 6 (2016).

[34] A.M. Beale, G. Sankar, Understanding the crystallization of nanosized cobalt aluminate spinel from ion-exchanged zeolites using combined *in situ* QEXAFS/XRD, *Chem. Mater.* 18 (2006) 263–272.

[35] G. Zhang, F. Liu, H. Liu, J. Qu, R. Liu, Respective role of Fe and Mn oxide contents for arsenic sorption in iron and manganese binary oxide: an X-ray absorption spectroscopy investigation, *Environ. Sci. Technol.* 48 (2014) 10316–10322.

[36] P.L. Meena, R. Kumar, K. Sreenivas, Rietveld refinement and spectroscopic analysis of Co_{3-x}Mn_xO₄ (0.1 ≤ x ≤ 1.0) ceramic compositions, *Int. J. Phys. Chem. Math. Sci.* 3 (2014) 7.

[37] C.S. Swamy, S. Kannan, Y. Li, J.N. Armor, T.A. Braymer, US Patent 5,407,652, 1995.

[38] J. Pérez-Ramírez, J.M. García-Cortés, F. Kapteijn, M.J. Illán-Gómez, A. Ribera, C. Salinas-Martínez de Lecea, J.A. Moulijn, Dual-bed catalytic system for NO_x-N₂ removal: a practical application for lean-burn deNO_x HC-SCR, *Appl. Catal. B Environ.* 25 (2000) 191–203.

[39] X. Xu, X. Xu, G. Zhang, X. Niu, Preparation of Co-Al mixed oxide-supported gold catalysts and their catalytic activity for N₂O decomposition, *J. Fuel Chem. Technol.* 37 (2009) 595–600.

[40] K. Karášková, L. Obalová, K. Jirátová, F. Kovanda, Effect of promoters in Co-Mn-Al mixed oxide catalyst on N₂O decomposition, *Chem. Eng. J.* 160 (2010) 480–487.

[41] T.S. Farris, Y. Li, J.N. Armor, T.A. Braymer, US Patent 5,472,677, 1995.

[42] M. Konsolakis, Recent advances on nitrous oxide (N₂O) decomposition over non-noble-metal oxide catalysts: catalytic performance, mechanistic considerations, and surface chemistry aspects, *ACS Catal.* 5 (2015) 6397–6421.

[43] M. Jabłońska, L. Buselli, M. Nocuń, R. Palkovits, Silver-doped cobalt (magnesium) aluminum mixed metal oxides as potential catalysts for nitrous oxide decomposition, *ChemCatChem* 10 (2018) 296–304.

[44] S.A.C. Carabineiro, E. Papista, G.E. Marnelos, P.B. Tavares, F.J. Maldonado-Hódar, M. Konsolakis, *Mol. Catal.* 436 (2017) 78–89.

[45] P. Vanýsek, Electrochemical series, in: D.R. Lide (Ed.), *CRC Handbook of Chemistry and Physics*, 83rd ed., CRC Press, Boca Raton, 2002, pp. 8-21-8-31.